Applied Physics Express



# Optically transparent metasurfaces based on ITO: Numerical design and measurements in THz domain

To cite this article before publication: Suling SHEN *et al* 2020 *Appl. Phys. Express* in press https://doi.org/10.35848/1882-0786/abb641

# Optically transparent metasurfaces based on ITO: numerical design and measurements in THz domain

Suling Shen[1,2], Qiang Liu[3], Xudong Liu[1], Jialiang Huang[1], Mingyang Jia[1], Junle Qu[2], Yaochun Shen[4], Yiwen Sun[1,*]

[1]*National-Regional Key Technology Engineering Laboratory for Medical Ultrasound, Guangdong Key Laboratory for Biomedical Measurements and Ultrasound Imaging, Department of Biomedical Engineering, School of Medicine, Shenzhen University, Shenzhen 518060, China*

[2]*College of Physics and Optoelectronic Engineering, Shenzhen University, Shenzhen 518060, China*

[3]*Department of Biomedical Engineering, Southern University of Science and Technology, Shenzhen 518055, China.*

[4]*Department of Electrical Engineering and Electronics, University of Liverpool, Liverpool L69 3GJ, UK*

* E-mail: ywsun@szu.edu.cn

Complementary split-ring resonators (CSRRs) metasurfaces present interesting applications in terahertz biosensing. Indium tin oxide (ITO) is an essential optoelectronic material because of optical transparency, high conductivity and good stability. In this letter, we innovatively suggest that ITO-based CSRRs metasurface can excite multi-peaks resonance in 0.1-2 THz by numerical simulation and experimental measurements. The multi-peak-resonance presents red-shift characteristics with increasing the external radius of the split-ring. The experimental results are in close agreement with the numerical values, which may indicate that the proposed ITO-based CSRRs metasurface may play a significant role in visible terahertz bio-sensing applications.

Over the past decades, terahertz (THz) radiation has attached intensive research interest because of its unique properties in this electromagnetic spectral range (1 THz=$10^{12}$ Hz). THz metasurface, which is an artificial subwavelength structure with extraordinary electromagnetic response in THz radiation, has been extensively explored for a wide range of application fields, such as wave beam shaper, waveguide, and modulator [1-5]. Meanwhile, it also has potential applications in the biomedical research as a biosensor by taking advantage of plasmonic resonances to enhance sensitivity [6-8]. The first metasurface designed for bio-sensing applications was proposed by Brolo et al in 2004 [9]. This research was extended to THz frequency in 2007 by Debus et al. [10]. After that, research into THz bio-sensing technology relating to metasurface has attracted considerable attention. Singh's group developed a flexible terahertz metamaterial sensor on a low refractive index substrate [11]. Xie's group demonstrated graphene-gold heterostructure terahertz metamaterial sensor with ultrahigh sensitivity [12]. Okamoto et al. have reported a terahertz sensor using photonic crystal cavity with record-high Q factor of 10000 [13]. However, most materials studied for metasurface so far are exclusively limited to common metal (Au, Ag, Al, Cu) [9], graphene [12] and silicon [14]. Unfortunately, these materials have drawbacks including high-cost, low-biocompatibility, poor reusability and instability, which restricted their practical applications in THz bio-sensing [15-16].

ITO is an n-type degenerate semiconductors with wide band-gap (≥3 eV) [17-19]. The good biocompatibility [20] and THz plasmonic response [17, 21] make ITO an attractive candidate for THz metasurface bio-sensing. Furthermore, the demand for highly optically transparent bio-sensing continues to grow in many practical applications because it makes the sensing process visible to the naked eye and allows visible light photosensitive sensing [22]. Concretely, photodynamic therapy is one kind of drug/instrument combination therapy technology which causes cell necrosis, apoptosis, autophagy by irradiating tissue/cells with light at specific optical wavelength. But, there is limited way to dynamically monitor the process of photodynamic therapy and accurately assess the curative effect. Optically transparent ITO-based THz metasurface may become suitable for such purpose by providing a transparent platform for the simultaneous implementations of photodynamic therapy [23] and THz bio-sensing [24]. Besides, optically transparent ITO-based metasurface is very promising for photoacoustic imaging of melanoma cells by providing lower noises compared to metallic metasurface [25]. However, there has been few report on the ITO metasurface for optically transparent bio-sensing in THz field.

Fluorine-doped Tin Oxide (FTO) shows very similar optoelectronic properties with ITO [26]. With the purpose to make a comparison, numerical simulations were carried out to study the performance of both ITO and FTO based CSRRs metasurfaces. This letter is organized as follows. We first designed a type of CSRRs metasurfaces with ITO and FTO respectively. Then, we described numerical simulation of the reflection, transmission, absorption and electric distribution in the 0.1-2 THz based on the Drude models of ITO. In section 2, the design of ITO-and FTO-based CSRRs metasurfaces are presented. In section 3, characteristics of the proposed CSRRs metasurface, such as reflection, transmission, absorption, magnetic field distributions are analyzed and discussed. In section 4, the experimental results on transmission and reflection are processed and compared. Conclusions are in section 5.

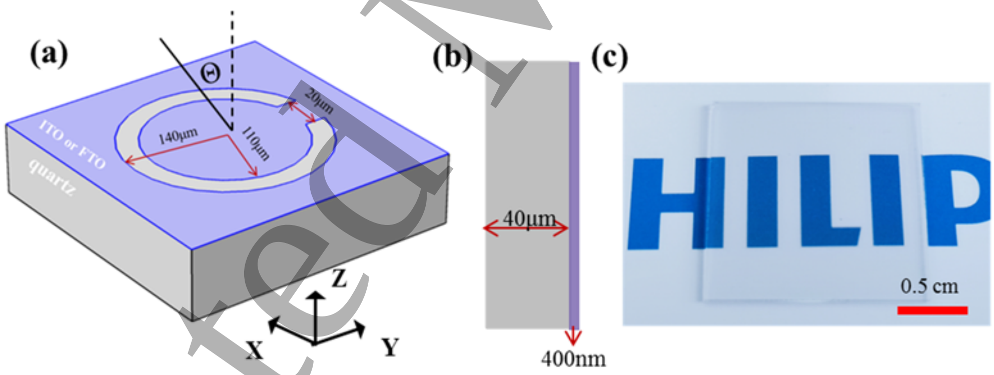


Fig. 1: (a) Schematic of ITO or FTO CSRRs metasurfaces: here the purple and gray colors denote ITO or FTO thin film, and quartz substrate respectively; (b) Schematic of cross section view of (a); (c) Excellent optically transparent sample of ITO CSRRs metasurface on quartz substrate.

We investigate the CSRRs metasurface consisting of quartz substrate and thin film ITO or FTO. The geometry is shown in Fig. 1 (a) and (b). The external and the internal radius of the split-ring is 140 μm and 110 μm respectively; and the gap width, which is completely open on one side of the ring, is 20 μm. The CSRR is considered to be distributed periodically, while the lattice constant is assumed to be 400 μm. Periodic boundary conditions have been applied for calculating the transmission (T), reflectivity (F) and absorption (A) of a single unit of CSRR. The thickness of ITO (FTO) is 400 nm while the thickness of the quartz substrate is 40 μm. THz wave is assumed to have normal incidence to the metasurface. The aforementioned CSRRs comes from the Babinet's principle in which the admittance of CSRRs goes to infinite and there is a total transmission, where CSRRs can be considered as quasi-static LC resonators. CSRRs based on ITO and FTO may provide a convenient way for controlling the position of resonance peak by using different radius of the split-ring [27-30]. The sample of ITO CSRRs metasurface on quartz substrate is shown in Fig. (c). It can be observed that the sample presents excellent optical transparency.

The following simulations on numerical analysis of electromagnetic response based on ITO and FTO CSRRs metasurface are performed by using finite-element method (FEM) as provided by COMSOL Multiphysics. In the following, two perfectly matched layers (PML) are applied in the top and bottom layers of the modeling region. The propagation direction of the EM field is perpendicular to the metallic patch, and the incident magnetic field $H_0$ is parallel to the x axis.

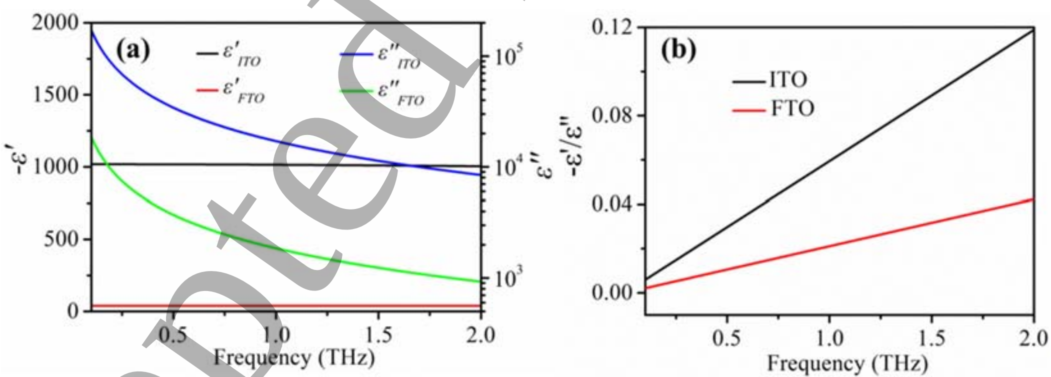


Fig. 2: (a) The real part $\varepsilon'$ and the imaginary part $\varepsilon''$ of the permittivity of ITO and FTO at 0.1-2 THz; (b) The frequency-dependent ratio $-\varepsilon'/\varepsilon''$ of ITO and FTO at 0.1-2 THz. The complex dielectric constant was calculated using the parameter of $\varepsilon_\infty$ equal to 4.4, $\omega_p$ equal to $1.606\times10^{15}$ rad/s, $\tau$ equal to 9.5 fs for ITO [29] and $\varepsilon_\infty$ equal to 3.85, $\omega_p$ equal to $1.78\times10^{15}$ rad/s, $\tau$ equal to 3.69 fs for FTO [26]. Following the parameters provided in refs. [24,27], the calculated skin depth of ITO (FTO) is found to be at the

regime 0.75 μm ~ 3 μm (0.8 μm ~ 3.8 μm), provided with that the frequency of THz wave lies within 0.1 THz ~ 2 THz.

The frequency-dependent permittivity of a conductor can be described using the Drude model:

$$\varepsilon = \varepsilon_\infty - \frac{(\omega_p / \omega)^2}{1 + i / \omega\tau} \tag{1}$$

$$\omega_p^2 = \frac{ne^2}{m_{\text{eff}}\varepsilon_0} \tag{2}$$

where $m_{\text{eff}}$ is effective mass of the electrons, $\varepsilon_\infty$ is the high-frequency dielectric constant, $\varepsilon_0$ is the vacuum dielectric constant, $N$, $\tau$ and $\omega_p$ present the electron density, scattering time and the plasma frequency respectively.

Based on the computation for CSRRs metasurfaces, the calculated real part $\varepsilon'$ and the imaginary part $\varepsilon''$ of the permittivity of ITO are both larger than that of FTO in the range of 0.1 to 2 THz as depicted in Fig. 2 (a). Meanwhile, the more metallic behavior is demonstrated by increasing frequency-dependent ratio of $-\varepsilon'/\varepsilon''$ of ITO than that of FTO [30], as shown in Fig. 2(b). The result suggests that ITO should exhibit better electric field behavior than FTO discussed in section 3 which exactly explains why ITO possesses better sensing performance than FTO in THz range.

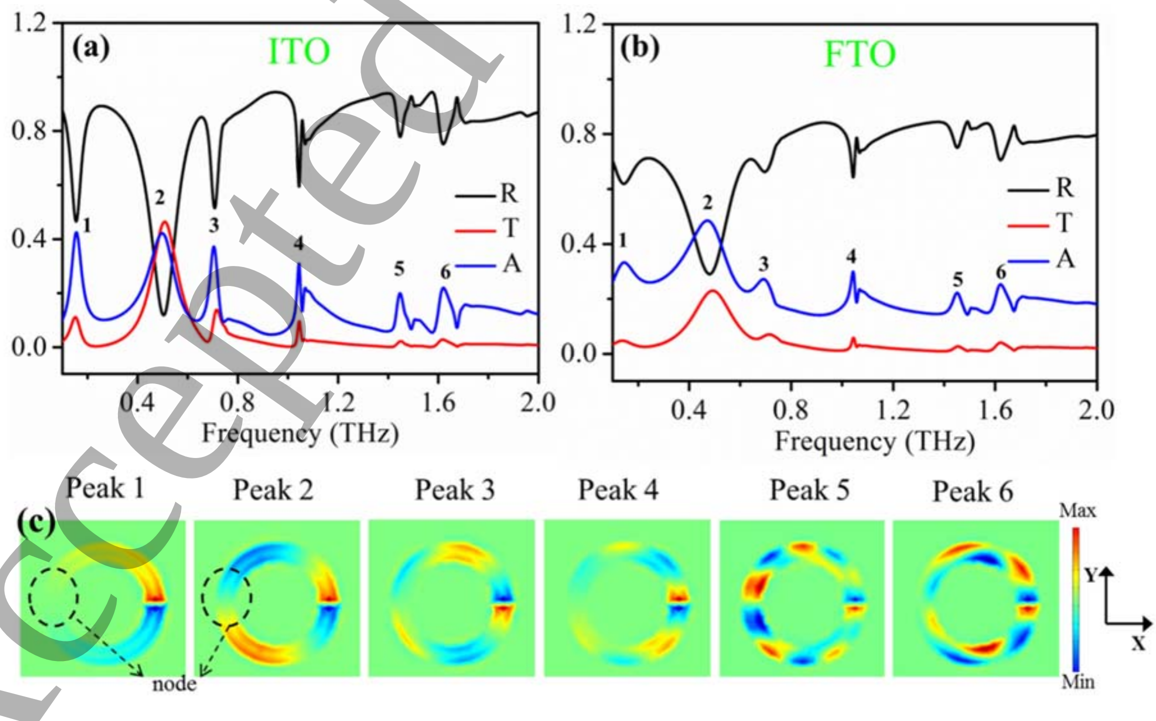

Fig. 3: The computed frequency-dependent reflection, transmission and absorption of (a) ITO and (b) FTO CSRRs metasurfaces by normal incidence. (c) The distributions of magnetic flux density $B_z$ of ITO-based CSSRs corresponding to peaks 1- 6.

Fig. 3 (a, b) show the computed frequency-dependent reflection, transmission and absorption of the ITO and FTO CSRRs in 0.1-2 THz. The reflection (R) and transmission (T) are the ratio of the magnitude of the electric field of the reflected wave $E_{ref}$ and transmitted wave $E_{tra}$ to that of the incident plane wave $E_{in}$ respectively, while the absorption (A) can be expressed by: A = 1－R－T. There are 6 resonance peaks for both ITO and FTO metasurfaces in the range of 0.1-2 THz. This multi-resonances characteristic will help to achieve a wide analyte refractive index range with competitive resolution and has potential for multi-analyte sensing and self-reference [31]. The origin of these peaks may be attributed by the excitation of plasmonic (or photonic) eigenmodes in the micro-structures of ITO/FTO thin films. It can be observed that FTO-based CSRRs present the broader resonance peaks because of its higher dielectric loss (see Fig. 2a). We thus demonstrate the feasibility of applying ITO-based CSSRs metasurface for bio-sensing mentioned in the supplementary data. The eigen-mode of peak 2 for both ITO- and FTO-based CSRRs shows the highest resonance peak, such phenomenon may be relevant to the lowest effective refractive index of plasmonic eigen-mode, which will be discussed in the following section.

To gain a better understanding toward the mechanism that governing the appearance of multi-peaks as shown in Fig. 3 (a, b), we have also provided the distributions of magnetic flux density $B_z$ of ITO-based CSSRs corresponding to peaks 1- 6 in Fig. 3(c). According to the Babinet's priciple [27], there exists a electric current density $J_x$ at the gap region, as a result, the magnetic flux density $B_z$ at the upper and lower edges of the gap demonstrates positive and negative signs, respectively. Due to the electromagnetic oscillation that incorporated with the Fabry-Perot nature of the split ring, the arm of CSRR demonstrates standing wave patterns. Considering the similar resonance response of ITO and FTO, we only focus on the discussions on ITO-based CSRRs in this section. It can be observed that standing waves with varied number of nodes are found to be perpendicular to the cross-sectional plane. More specifically, there exists a single number of node in the magnetic flux density $B_z$ for peak 1; while increasing number of nodes of magnetic flux density $B_z$ can be found for peaks 2 to 6.

According to Babinet's principle, resonant peaks of 1-3 are associated with plasmonic egien-modes. Therefore, it is desirable to calculate the real part of the effective refractive index $Re(n_{eff})$ of each plasmonic egien-mode for sensing-related applications by the following the equation [32]:

$$L_{eff} = \begin{cases} \dfrac{\lambda_0}{\mathrm{Re}(n_{eff})}, & m = 1 \\ \dfrac{m}{2}\dfrac{\lambda_0}{\mathrm{Re}(n_{eff})}, & m = 3, 5, \ldots \end{cases} \quad (3)$$

$$L_{eff} = L - g \quad (4)$$

where $L_{eff}$ is the effective length of the split ring resonator, $L$ is the perimeter of the ring as expressed by $L = 2\pi\,(R_{external} - w/2)$ (note that $R_{external}$ is the external radius of the split-ring, and $w$ is the difference between external radius and internal radius of the split-ring), $g$ is the gap of the split-ring, $\lambda_0$ is the incident wavelength in the vacuum, $m$ is the number of magnetic flux density $B_z$ nodes as distributed in the split ring arm. Table 1 has summarized the effective refractive indices of peaks 1 to 3. While for the cases of peaks 4-6, the size of a CSRR unit cell is 400 μm, which is comparable to the incident wavelength of THz wave, e.g. approximately 300 μm associated with the peak 4. This will cause optical diffraction. Therefore, the appearance of peaks 4-6 may be explained by the diffraction effect of THz wave.

Table1: Effective refractive indices of mode 1 to 3

| **Paramters** | **Peak 1** | **Peak 2** | **Peak 3** |
|---|---|---|---|
| Resonant-frequency/THz | 0.1573 | 0.5010 | 0.7050 |
| Number of $B_z$ nodes $m$ | 1 | 3 | 5 |
| Effective refractive index | 2.4918 | 1.1735 | 1.3898 |

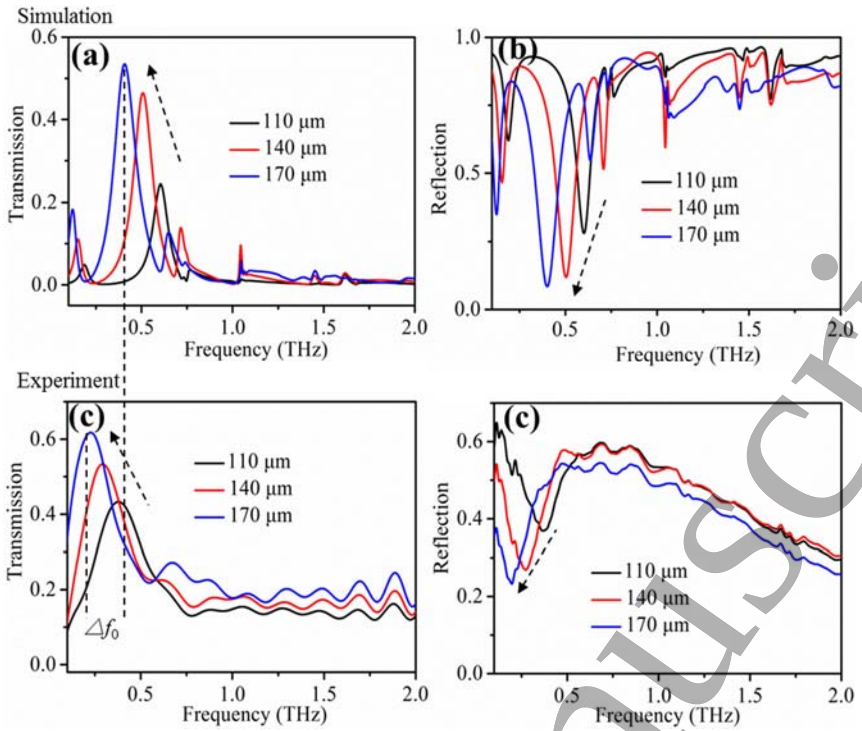


Fig. 4: CSRRs radius-dependent transmission (a) and reflection (b) based on ITO, results are obtained by finite element method; CSRR radius-dependent transmission (c) and reflection (d) based on ITO, results are obtained by experimental measurement.

Here, we first examine how CSRRs radius affects initial position of resonance peaks based on ITO metasurface by simulation. Fig. 4 provides the simulation data on CSRRs radius-dependent transmission (a) and reflection (b). For peaks 1-3 (in 0.1-1THz), both transmission and reflection red shift evidently after increasing the external radius of the split-ring. The red-shift of resonant frequency can be explained by the LC-related equations provided by [33]: the increased the external radius of the split-ring causes the decrease of resonance frequency. While for peaks 4 - 6, the resonant frequency has no obvious shift, potential reasons may be described as: due to the increased ratio of the thickness of ITO to the corresponding operational wavelength, peaks 4 - 6 partially violate the Babinet's priciple. In addition, the associated wavelength of peaks 4 - 6 is comparable to the size of a CSRR unit cell, the diffraction effect may thus play the dominant role in the spectral response of peaks 4 - 6.

Here, we also examine experimentally the effect of the ring radius on the initial position of resonance peaks based on ITO CSRRs metasurface. Fig. 4 (c) and (d) provides the measurement data of transmission and reflection based on different ITO CSRRs radius. It can be observed that the main peaks (in 0.1-1THz) of both transmission and reflection red-shift evidently after increasing the external radius of the split-ring which is consisted well with simulation results. The adjustable characteristics of resonance peaks according to ITO CSRRs radius make ITO more flexible and practical as visible terahertz biosensor candidate.

Fig. 4 (a, c) compares the simulation and experimental results. It can be observed that the experiment data present high-quality resonance peaks in both transmission and reflection in 0.1-1 THz which are consistent with the simulation results. However, the resonance frequency of both transmission and reflection are red shifted compared with simulation data. In addition, the measurement results show no obvious resonance peaks in the range of 1-2 THz. The experimental results show a little discrepancy with the simulation results owing to the difference between the permittivity and conductivity of ITO used in simulation taking from literature [29] and in experiment processed by lithography technology. The relatively in-sufficient references that can provide experimental data on permittivity and conductivity of ITO/FTO at varied thickness and doping concentrations may hinder the further investigation; however, our simulation results may provide basic reference and guidance for the future design and relevant optimization of ITO- and FTO-based metasurfaces.

In summary, we have first designed both ITO- and FTO-based CSRRs metasurfaces and made a preliminary exploration on the electromagnetic response of such two designs. ITO-based CSRRs metasurfaces were detected by THz-TDS system in transmission and reflection geometry. Mechanisms that may govern the existence of multi-peaks, the spectral-shift ~~in terahertz transmission, reflection and absorption~~ have been provided. Good agreement between numerical simulation and experimental results, as combined with excellent optical transparency, the proposed ITO-based CSRRs metasurfaces may find wide applications in visualization of bio-medical operation and micro-fluid implementation in THz range.

**Acknowledgements**

The authors gratefully acknowledge partial financial support for this work from the National Natural Science Foundation of China (61805148, 61975135, 61275043, 61605128), International Cooperation and Exchanges NSFC (61911530218), SZU Start-up Fund (85304-00000334), Shenzhen High-end Talent Research Start-up Fund (827-000366), Shenzhen International Scientific and Technological Cooperation Project (GJHZ20190822095407131), Basic and Applied Basic Research Foundation of Guangdong Province (2019A1515111007) and Natural Science Foundation of Guangdong Province (2017A030310455, 2019A1515010869).

**References**


1. D. R. Smith, W. J. Padilla, D. C. Vier, Physical review letters 84(18), 4184-4187 (2000).
2. N. Yu, F. Capasso, Nature materials 13(2), 139-150 (2014).
3. M. Gupta, R. Singh, Advanced Optical Materials 8(12), 1902025-1902032 (2020).
4. R. Singh, W.Cao, I. Al-Naib, L.Cong, W. Withayachumnankul, W. Zhang, Applied Physics Letters 105(17), 171101-171121(2014).
5. Y.K. Srivastava, R. T. Ako, M.Gupta, M. Bhaskaran, S. Sriram, R. Singh, Applied Physics Letters 115(15), 151105-151122(2019).
6. K. Shih, P. Pitchappa, L. Jin, C.H.Chen, R. Singh, C. Lee, Appl. Phys. Lett. 113(7), 071105-071111 (2018).
7. J. F. O'Hara, R. Singh, I. Brener, E. Smirnova, J. Han, A. J. Taylor, W. Zhang, Optics Express 16 (3), 1786-1795 (2008).
8. M. Gupta, Y. K. Srivastava, M. Manjappa, R. Singh, Appl. Phys. Lett. 110(12), 121108- 121114(2017).
9. A. G. Brolo, R. Gordon, B. Leathem, K. L. Kavanagh, Langmuir 20(12), 4813-4815(2004).
10. C. Debus, P. H. Bolivar, Appl. Phys. Lett. 91(18), 184102-184104 (2007).
11. Y. K. Srivastava, L. Cong, R. Singh, Applied Physics Letters 111 (20), 201101-201107(2017).
12. W. Xu, L. Xie, J. Zhu, L. Tang, R. Singh, C. Wang,Y. Ma, H.T. Chen, Y. Ying, Carbon 141, 247-252 (2019).
13. K. Okamoto, K. Tsuruda, S. Diebold, S. Hisatake, M. Fujita, T. Nagatsuma, J Infrared Milli Terahz Waves 38, 1085–1097 (2017).
14. J. Lee, J. Yoon, M. Jung, J. Hong, S. Song, R. Magnusson, Appl. Phys. Lett. 104(23), 233505- 233509(2014).
15. F. Yan, L. Li, R. Wang, H. Tian, J. Liu, J. Liu, F. Tian, J. Zhang, Journal of Lightwave Technology 37(4), 1103-1112 (2019).

16. B. Ruan, J. Guo, L. Wu, J. Zhu, Q. You, X. Dai, Y. Xiang, Sensors 17(8), 1924-1933 (2017).

17. A. S. Thampy, S. K. Dhamodharan, Physica E 66, 52-58 (2015).

18. S. Shen, L. Gao, C. He, Z. Zhang, Q. Sun, Y. Li, Organic Electronics 14, 875–881(2013).

19. A. K. Sahoo , C. Yang , O. Wada, IEEE Transactions on Terahertz Science and Technology 9 (4), 399-408 (2019).

20. A. María, F. Xiomara, G. Albert, D. Francesco, H. Alejandro, B. Jordina, R.Javier, Lab on Chip 15, 2568-2580(2019).

21. J. Wang, Y. Deng, Y. Wu, S. Lai , W. Gu, Journal of Infrared, Millimeter, and Terahertz Waves 40,648-656(2019).

22. Y. Lee, B. Choi, J. Yoon, Y. Kim, J. Park, H. J. Kim, D. H. Kim, D. M. Kim, S. Kim, S. J. Choi, AIP Advances 8, 065109-065115 (2018).

23. X. Zheng, Z. Xiao, X. Ling, J Mater Sci: Mater Electron 28, 7739–7744 (2017).

24. X. Zhao, Z. Lin, Y. Wang, X. Yang, K. Yang, Y. Zhang, J. Peng, M. L. Hapelle, L. Zhang, W. Fu, Biomedical Optics Express 10, 1196-1206 (2019).

25. Q. Chen, H. Guo, T. Jin, W. Qi, H. Xie, L. Xi, Optics Letters, 43(7), 1615-1618 2018).

26. K. Farnood, O. Isaiah, W. Justin, N. Nima, N. Janardan, R. Imen, E. Robert, Optical Materials Express 5 (10), 2184-2192 (2015).

27. L. Zhang, T. Koschny, C. M. Soukoulis, Physical Review B 87, 045101 (2013).

28. M. Beruete1, M. Aznabet, M. Navarro-Cía, O. El Mrabet, F. Falcone1, N. Aknin, M. Essaaidi, and M. Sorolla, Optics Express 17(3), 1274-1281 (2008).

29. N. Wolf, D. Gerstenlauer and J. Manara, Journal of Physics: Conference Series 395, 012064 (2012).

30. V. N. Gururaj , M. S. Vladimir, and B. Alexandra, Adv. Mater 25, 3264–3294 (2013).

31. N. D. Gómez-Cardona, E. Reyes-Vera, P. Torres, IEEE Sensors 18, 7492-7498 (2018).

32. G. Wei, J. Tian, R. Yang, Optik - International Journal for Light and Electron Optics 193, 162990- 163001(2019).

33. O. Sydoruk, E. Tatartschuk, E. Shamonina, L. Solymar, Journal of Applied Physics 105, 014903-014907 (2009).